Astron. Astrophys. 346, 586–598 (1999)

ASTRONOMY AND ASTROPHYSICS

Photometric parameters for rotating models of A- and F-type stars

F. Pérez Hernández[1], **A. Claret**[2], **M.M. Hernández**[1], **and E. Michel**[3]

[1] Instituto de Astrofísica de Canarias, E-38200 La Laguna, Tenerife, Spain
[2] Instituto de Astrofísica de Andalucía, E-18080 Granada, Spain
[3] DASGAL, URA CNRS 335, Observatoire de Paris, F-92195 Meudon, France

Received 19 November 1998 / Accepted 26 March 1999

Abstract. We have computed the photometric magnitudes of rotating atmospheres–based on the simple model of Collins–for a grid suitable for main-sequence and slightly evolved stars of spectral type A0 to F5. A gravity-darkening law valid for radiative and convective envelopes has been considered. The general results are given as magnitude differences between rotating and non-rotating copartners to allow for the use of any photometric calibration. A simple interpolation on these results gives the photometric parameters for interior rotating models but we also indicate how they can be used to correct for the effect of rotation when an investigation with non-rotating models is carried out. We illustrate the procedure with the interesting case of the Praesepe Cluster.

Key words: stars: rotation – stars: fundamental parameters – stars: variables: δ Sct – Galaxy: open clusters and associations: individual: Praesepe

1. Introduction

This article deals with the relation between global parameters of fast rotating F and A stars and their photometric parameters. It was first conceived in the framework of the asteroseismology of δ Scuti stars. In particular, in a recent work, Michel et al. (1999) and Hernández et al. (1998) analysed several δ Scuti stars in the Praesepe Cluster and attempted to obtain information on such stars from their modes of oscillation. As in other works, it was clear that the seismological analysis must be accompanied by the most accurate possible estimates of the stellar parameters. Since most of these stars are fast rotators, this is not a simple task and, as shown by Michel et al. (1998, 1999), the inclusion of the photometric effect of rotation on the location of the stars in the colour–magnitude diagram can by no means be neglected.

A method for computing the emergent flux from a rapidly rotating star was given by Collins (1963). Some important improvements were developed by Collins (1965, 1966), Hardorp & Strittmatter (1968) and Maeder & Peytremann (1970, 1972). The latter authors included spectral lines in their atmospheric models, developing the most consistent calculations up to that time. Michel et al. (1999) used the results of Maeder & Peytremann (1970) for estimating the location of the δ Scuti stars of the Praesepe Cluster. But these computations were limited to very few models and have to be updated.

Collins & Sonneborn (1977) reported extensive calculations for photometric parameters in the Strömgren system for ZAMS stars. In some recent work (Annamma & Rajamohan 1992; Figueras & Blasi 1998) these results have been used for different applications. Finally, concerning the improvements in the determination of the photometric effect of rotation, we need to mention the work by Collins & Smith (1985), who used proper atmospheric and interior models, and extended previous work in two ways: i) not only uniform rotation, as in other studies, but also differential rotation constant on cylinders was considered; ii) they obtained statistical results for an ensemble of stars in an attempt to compare with the observed properties of galactic clusters. Unfortunately the results reported in this paper are not of direct use for our purposes because we wish to examine the effect for isolated stars. The work of Collins & Smith (1985) was also limited to ZAMS models.

In recomputing the photometric effect of rotation, we have used up-to-date models but we have also considered the gravity-darkening law given by Claret (1998), primarily developed for the interpretation of the light curves of eclipsing binaries. To our knowledge, all previous work on the photometric effect of rotation has been limited to the von Zeipel law, which is strictly valid only for stars with full radiative envelopes. The whole method is summarized in Sect. 2.1.

The location of a fast rotating star in a photometric diagram depends on the atmospheric and the interior models used. It was common in previous work to give the results after taking both into account, but, as explicitly shown in the present paper, the emergent flux of a rotating star can be fixed to a good approximation by giving two quantities, $g_{\rm e}$ and $T_{\rm e}$ (that replace g and $T_{\rm eff}$ of spherical stars) and the composition. In Sect. 2.2 we report results in such a grid. This can be very useful because it allows the location of the stellar models in the photometric diagrams to be determined based on any desired rotating interior model that includes shape distortion. On the other hand, the results given in Sect. 2.2 can still be used in a rather straightforward way for computations based on spherically symmetric, rotating and non-rotating, interior models as we shall describe in Sect. 2.3.

Send offprint requests to: F. Pérez Hernández (fph@ll.iac.es)

In Sect. 3 we consider, as an example, the problem of isochrone fits in the Praesepe Cluster and return to our original problem of determining the global parameters of associated non-rotating models, suitable for a theoretical analysis of some properties of δ Scuti stars.

We finish this introduction by drawing attention to an important point related to the photometric effect of rotation, which, although beyond the scope of the present paper, must be borne in mind. In most cases the only observational parameter concerning the rotation of the star is $v \sin i$, which can be determined from the shape of certain spectral lines. For slowly rotating stars the method originally suggested by Shajn & Struve (1929), which take into account the kinematic effect of rotation on line broadening, can be used. For fast rotating stars, shape distortion and gravity-darkening affect the line profiles as shown by Collins (1974). Slettebak et al. (1975) estimated values of $v \sin i$ for a sample of stars taking into account this effect. In principle the effect of shape distortion and gravity-darkening is interesting because, at least formally, it can be used to determine v and i separately from the observations since a variation in line broadening when comparing ultraviolet and visual line profiles is expected. Carpenter et al. (1984) perform such a comparison for late-B and A-type stars.

2. Photometric magnitudes for rotating models

In this section we shall compute the differences in the photometric magnitudes between uniformly rotating and non-rotating models for a grid suitable for main sequence and slightly evolved stars of spectral type A0 to F5. Later on we shall define what we mean by rotating and non-rotating copartners. Although the method used is basically that of Collins (1963)–see also Collins & Smith (1985) and references therein–we have found it convenient to summarize the entire procedure rather than limit the discussion to our modifications. This will also help us to justify the way in which the results are given.

We start with a qualitative description of the photometric effect of rotation. An isolated star whose rotational motion is completely negligible can, in most cases, be approximated as a spherical configuration, the isobaric surfaces being described by means of concentric spheres. The temperature, density and gravitational potential also possess spherical symmetry. However, if the star rotates about a fixed axis in space with a pronounced angular velocity, it then becomes an oblate figure. The isobaric and the isopycnic (equal density) surfaces do not necessarily coincide unless the rotation is uniform or constant over cylinders centred about the axis of rotation (Poincaré–Wavre theorem, see, e.g., Tassoul 1978). For barotropic models (for which a relation of the form $p = p(\rho)$ exists) this must be the case. On the other hand, non barotropic models for which rotation is assumed to be uniform or constant on cylinders are called pseudo-barotropes. For such models, the surfaces of constant effective potential, pressure, density and, if composition is uniform, temperature, all coincide. The effective gravity is orthogonal to such equipotential surfaces. For uniform rotation, the effective gravity is larger at the poles than at the equator and hence the same follows for the temperature gradient. Therefore, the flux (radiative or convective), which increases with the temperature gradient, is also larger at the poles than at the equator. The same follows for the effective temperature by virtue of Stefan's law. This is the gravity-darkening effect. In addition a star seen pole-on has a larger projected area than a equator-on star. Therefore, a star which is seen pole-on will look brighter and hotter than the same star seen equator-on. In general, the position of the star in a colour–magnitude diagram depends not only on its intrinsic parameters but also on the angle i between the rotational axis and the line of sight. This geometrical effect, which includes shape distortion and gravity-darkening, will be discussed in Sects. 2.1 and 2.2.

On the other hand, since the centrifugal force is in general much smaller in the core of the star than in the external layers, the luminosity (the energy per unit time generated, mainly, in the core) decreases by a small fraction with respect to an otherwise equivalent non-rotating star while the mean radius increases by a significant amount. Thus, the mean effective temperature of a rotating star is smaller than that of its corresponding non-rotating object and hence, on average, rotation makes the stars appear redshifted in a colour–magnitude diagram. The photometric effect caused by changes in the interior structure will be briefly discussed in Sect. 2.3.

2.1. Basic assumptions and equations

Although the method of Collins can be applied to any barotrope or pseudo-barotrope, we shall limit our discussion to uniform rotation. Collins & Smith (1985) considered a rotational law with increasing angular velocity for increasing stellar latitude and found a larger effect than for rigid rotation, but the situation can be reversed if a law with decreasing angular velocity with increasing stellar latitude is considered. Therefore, uniform rotation can be regarded as a simple, one-parameter, intermediate case for which extensive but as yet manageable results can be reported.

In principle, the shape of a rotating star is unknown a priori and must be derived from the equations of stellar structure. However a great simplification is achieved by noting that for the uppermost layers of a star, a good approximation is to assume that the gravitational potential is that of a spherical configuration with the same mass. At least for uniform rotation, this result is supported by numerical calculations (e.g. Sackmann 1970; Papaloizou & Whelan 1973). In the following, this approximation will be used; that is, the surface of the star is assumed to be a Roche surface.

It is convenient to introduce dimensionless quantities. We define

$$\tilde{w} \equiv \frac{\Omega}{\tilde{\Omega}_{\rm c}} \ , \tag{1}$$

where Ω is the angular rotational velocity of the star and

$$\tilde{\Omega}_{\rm c}^2 \equiv \frac{8GM}{27R_{\rm p}^3} \ . \tag{2}$$

Here M is the mass and $R_{\rm p}$ the polar radius of the star. G is the gravitational constant. It can be shown that $\tilde{\Omega}_{\rm c}$ is the angular rotational velocity that a star with the same M and R_p would have if the centrifugal force balanced the gravitational attraction at the equator. Thus $\tilde{w} < 1$ for any stellar configuration.

We introduce the relative radius at colatitude θ by

$$x(\theta) = R(\theta)/R_{\rm p} \ , \tag{3}$$

where $R(\theta)$ is the distance from the surface to the centre at colatitude θ. It can be shown that, for a Roche surface, x is given by

$$x(\theta) = \frac{3}{\tilde{w}\sin\theta}\cos\left\{\frac{1}{3}\left[\pi + \arccos(\tilde{w}\sin\theta)\right]\right\} \tag{4}$$

(Harrington & Collins 1968). Thus the shape of the surface, $x = x(\theta)$, depends only on the relative angular velocity, $\tilde{w}$.

Under the same assumptions (uniform rotation and approximating the gravitational potential by that of a mass point), the effect on the hydrostatic equilibrium equation is to replace the gravitational potential by the effective potential

$$\phi = -\frac{GM}{R} - \frac{1}{2}\Omega^2 R^2(\theta)\sin^2\theta \ . \tag{5}$$

From this and Eq. (3) is easy to show that the modulus of the corresponding effective gravity is given by

$$g(\theta) = \frac{GM}{R_p^2} g_{\rm n}(\theta) \ , \tag{6}$$

where

$$g_{\rm n}(\theta) =$$

$$\frac{8}{27}\sqrt{\left(\frac{27}{8x^2} - \tilde{w}^2 x\sin^2\theta\right)^2 + \left(\tilde{w}^4 x^2\cos^2\theta\sin^2\theta\right)} \tag{7}$$

is a normalized effective gravity (Collins 1965). At a given colatitude, θ, $g_{\rm n}$ depends only on $\tilde{w}$.

At each point on the surface, we shall assume that the atmosphere can be approximated by a plane–parallel atmosphere with constant flux. Also at each point, we assume hydrostatic support under constant effective gravity. Thus, in this sense, we are dealing with classical atmospheric models. In particular, the emergent flux depends on $g(\theta)$, the effective temperature $T_{\rm eff}(\theta)$ and the composition (other parameters such as the turbulent velocity can be considered as well). This is a simplified model that, in particular, neglects the explicit effects of meridional circulations.

We shall now give an expression for $T_{\rm eff}(\theta)$. Here $T_{\rm eff}$ is defined by the Stefan's law $F = \sigma T_{\rm eff}^4$, where F is the emergent flux and σ is the Stefan–Boltzmann constant. We consider radiative transport first and assume the equation of diffusion for the transfer of energy. In this case the von Zeipel gravity-darkening law holds (see e.g. Tassoul 1978):

$$F \propto T_{\rm eff}^4 \propto g \ . \tag{8}$$

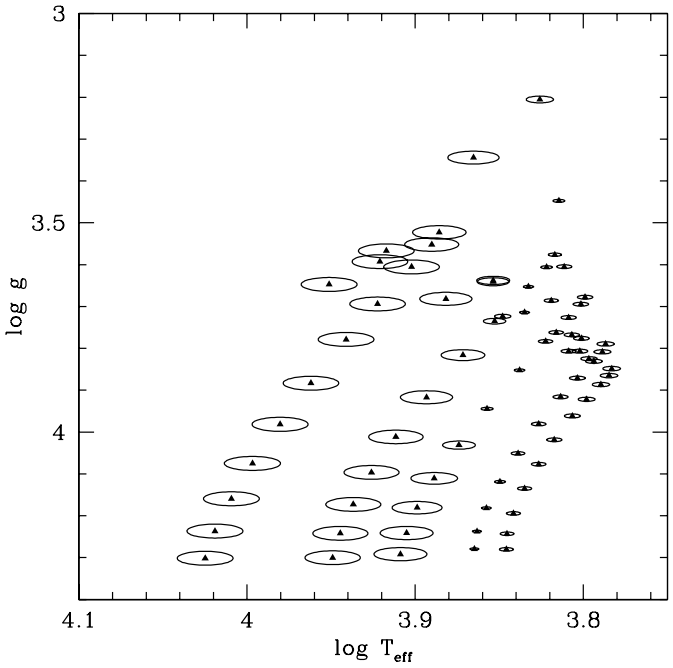

Fig. 1. Gravity-darkening exponent β for the five evolution sequences indicated in the text. The units are K and $\mathrm{cm\ s^{-2}}$ for $T_{\rm eff}$ and g, respectively. The models considered are indicated by triangles and β is proportional to the size of the corresponding ellipses.

As shown by Lucy (1967), for stars with convective envelopes the gravity-darkening law is approximately given by

$$F \propto T_{\rm eff}^4 \propto g^{0.32} \ . \tag{9}$$

In general the star will transport its energy both radiatively and convectively. In that case we can take a general law of the form

$$F \propto T_{\rm eff}^4 = C(\tilde{w}) g^{\beta} \ , \tag{10}$$

where $C(\tilde{w})$ and β are constants for a given rotating star. We have obtained the value of the gravity-darkening exponent, β, from the work by Claret (1998). The method developed in that paper makes use of evolutionary models and, for the first time, the gravity-darkening exponent is presented as a function of mass, age and chemical composition. The values of β derived by von Zeipel and Lucy for radiative and convective envelopes are then superseded and a smooth transition is achieved between both energy transport mechanisms.

In Fig. 1 we show in a $T_{\rm eff}$–g diagram, the values of β for five evolution sequences with solar metallicity and solar masses 1.5, 1.58, 1.78, 2.0 and 2.51, obtained directly from that work. The models are indicated by triangles and the size of the corresponding ellipses are proportional to β. The gravity-darkening exponent, β, depends on the envelope structure, but since we are going to consider stars in or just above the main sequence, we can assume to a good approximation that β depends only on $T_{\rm eff}$ and g, at least for fixed composition. For $\log(T_{\rm eff}) > 3.9$, where the envelopes are fully radiative, $\beta \simeq 1$; it sharply decreases down to $\beta \sim 0.15$ for lower effective temperatures–the precise value depending on g–and then rises to $\beta \approx 0.3$ at the red edge where the envelopes are convective.

Before continuing, we note the following problem. Consider a star with a fully radiative envelope, so that $\beta \simeq 1$ at the bottom of the atmosphere where the equation of diffusion holds to a good approximation. In our simple model, since $g(\theta)$ and $F(\theta)$ do not depend on depth, the value of β must be the same throughout the atmosphere. However, Smith (1970)–see also Smith & Worley (1974)–showed that under the same assumptions as above (in particular neglecting circulation) but using the Eddington approximation for the transfer equation, the gravity-darkening exponent takes the value $\beta = 0.46$. Since in the uppermost layers of the atmosphere this approximation for the radiative transport is better, our simple model, which must have constant β, cannot be completely satisfied. To solve this paradox, we follow Smith (1970) and consider meridional circulation to cause the flux to be constant over the atmosphere and equal to its value at the interior. Thus β is computed for envelope models and fixed for each model.

In Eq. (10), the constant $C(\tilde{w})$ can be expressed in terms of the intrinsic luminosity, L, by using the Stefan's law, $F = \sigma T_{\rm eff}^4$, and noticing that L is the integral of F over the stellar surface. Hence

$$C(\tilde{w}) = \frac{L}{\sigma}\left[\int_A g^\beta dA\right]^{-1} . \quad (11)$$

Here the integral is over the whole surface of area A.

By taking a Roche surface in Eq. (11), Eq. (10) can be expressed as

$$T_{\rm eff}^4(\theta) = \frac{L}{4\pi\sigma R_p^2} t_{\rm n}^4(\theta) , \quad (12)$$

where

$$t_{\rm n}^4(\theta) = g_{\rm n}^\beta \left[\int_0^1 \frac{g_{\rm n}^{\beta+1} x^4}{1-\frac{8}{27}\tilde{w}^2 x^3 \sin^2\theta} d(\cos\theta)\right]^{-1} \quad (13)$$

is a normalized effective temperature. At a given θ, $t_{\rm n}$ depends only on $\tilde{w}$.

Given $T_{\rm eff}(\theta)$ and $g(\theta)$, the monochromatic specific intensity, $I_\nu(\mu)$, at the top of the atmosphere can be obtained from a model (once the composition and other parameters are fixed). Here μ is the cosine of the angle between the line of sight and the normal to the surface. For a Roche surface, the value of μ at each point (θ, φ) can be computed for given i and $\tilde{w}$ by the expression

$$\mu = \frac{|\boldsymbol{g}\cdot\boldsymbol{i}|}{g} =$$

$$\frac{\left(1-\frac{8}{27}\tilde{w}^2 x^3\right)\sin i \sin\theta\cos\varphi + \cos i\cos\theta}{g_{\rm n} x^2} , \quad (14)$$

where $\boldsymbol{i}$ is a unit vector in the direction of the line of sight.

Once the specific intensity is known, the radiation emitted per unit frequency interval per steradian in the direction defined by the angle i can be computed from the expression

$$\mathcal{L}_\nu(\tilde{w}, i) = \int_A I_\nu(\mu)|\mu| dA , \quad (15)$$

where the integral is over the stellar surface of area A. For a uniformly rotating Roche surface it takes the form (Collins 1965)

$$\mathcal{L}_\nu(\tilde{w}, i) =$$

$$2R_{\rm p}^2 \int_0^{\pi/2}\int_0^{\pi} I_\nu(\theta,\varphi) x^2(\theta)\sin\theta f(\theta,\varphi) d\theta d\varphi , \quad (16)$$

where

$$f(\theta,\varphi) = \sin\theta\sin i\cos\varphi + \cos\theta\cos i -$$

$$\frac{8\tilde{w}^2 x^3(\theta)\sin\theta\cos\theta}{27-8\tilde{w}^2 x^3(\theta)\sin^2\theta}(\sin i\cos\varphi\cos\theta - \sin\theta\cos i) . \quad (17)$$

At each point on the surface f depends only on $\tilde{w}$ and i.

The function $\mathcal{L}_\nu(\tilde{w}, i)$ gives the spectrum of the star. Compared to that of a non-rotating star, not only the continuum but also the shape of the spectral lines is modified (e.g. Maeder & Peytremann 1970). This dynamical effect is included in our calculations. However, the Doppler shift due to rotation leaves the equivalent widths unchanged. Thus, it has no influence on the photometric measurements in which we are interested here and we have not taken it into account.

The integral of $\mathcal{L}_\nu$ over frequency ν would give the total radiation per steradian in the direction defined by the angle i (sometimes called the specific luminosity). This quantity gives the (specific) absolute bolometric magnitude, as would be derived from observations when corrected by distance. However we note that for rotating stars, $\mathcal{L}$ does not equal the intrinsic luminosity of the star; in particular, it depends on i.

In order to compare with photometric observations, filters must be considered. The integrated radiation for a given filter m with response function $T_{\rm m}(\nu)$ is given by

$$\mathcal{L}_{\rm m}(\tilde{w}, i) = B_{\rm m}\int_0^\infty T_{\rm m}(\nu)\mathcal{L}_\nu(\tilde{w}, i) d\nu , \quad (18)$$

where $B_{\rm m}$ is a calibration constant. From this equation the magnitudes and colours can be computed except for additive constants.

2.2. Differential photometric magnitudes

In general, to compare magnitudes and other photometric parameters calculated from atmospheric models with the observational ones, certain semi-empirical calibrations are required. In order to report results as independent as possible from such calibrations, we have split the problem in two. We compute the differences in magnitudes between rotating and non rotating models and then leave the problem of calculating absolute magnitudes for rotating models to the addition of the magnitudes of their non-rotating copartners as given by standard calibrations. Note that, at least formally, we assume that such semi-empirical calibrations are based on slowly rotating stars.

Assume we have a uniformly rotating model with mass M, intrinsic luminosity L and polar radius $R_{\rm p}$, rotating with angular

velocity Ω. Hence $\tilde{w}$ is fixed as well. We define the non-rotating copartner as a zero-rotation star with the same composition, mass, luminosity and a radius, R, numerically equal to $R_{\rm p}$.

It is important to note that these non-rotating copartners do not necessarily correspond to any self-consistent interior model. In fact, a family of models with the same input physics but different rotation rates would have different luminosities and polar radii. The non-rotating copartners defined above are only introduced to express the photometric results in terms of differences, such that they can be used, to a good approximation, with photometric calibrations other than the one considered here.

The difference in the magnitude in the filter m between the two models is given by

$$\Delta M_{\rm m}(\tilde{w},i) = -2.5\log\left[\frac{l_{\rm m}(\tilde{w},i)}{l_{\rm m}(0,i)}\right] \ , \qquad (19)$$

where

$$l_{\rm m}(\tilde{w},i) =$$

$$\int_0^\infty \int_0^{\pi/2} \int_0^{\pi} T_{\rm m}(\nu) I_\nu(\theta,\varphi) x^2(\theta) \sin\theta f(\theta,\varphi) d\theta d\varphi d\nu \ . \qquad (20)$$

Consider now a second rotating model with the same composition. If it has the same values of

$$g_{\rm e} \equiv \frac{GM}{R_{\rm p}^2} \qquad (21)$$

and

$$T_{\rm e} \equiv \frac{L}{4\pi\sigma R_{\rm p}^2} \ , \qquad (22)$$

then, from Eqs. (6) and (12), it follows that they have the same $g(\theta)$ and $T_{\rm eff}(\theta)$ for given $\tilde{w}$, and hence, taking into account expression (14), the same $I_\nu(\theta,\varphi)$ for given $\tilde{w}$ and i. Here we have assumed that both rotating models have the same β, which seems a good approximation as commented before. Furthermore, from Eq. (19) it follows that both rotating models will have the same magnitude difference, $\Delta M_{\rm m}(\tilde{w},i)$, as compared respectively to their non-rotating copartners. Thus we need only compute values of $\Delta M_{\rm m}(\tilde{w},i)$ for rotating models characterized by $T_{\rm e}$, $g_{\rm e}$ and composition. In particular, the results given in this section do not depend on other details of the rotating interior models. To those quantities the values of $M_{\rm m}$ for the non-rotating copartners, as defined above, must be added to obtain the absolute magnitudes of the rotating models.

The atmospheric models used are those of Kurucz (ATLAS9) for solar metallicity and $[M/H] = +0.2$. In principle, the specific intensity $I_\nu(\mu)$ at the top of the atmosphere must be computed at each point (θ,φ) taking atmospheric models with the corresponding values of $T_{\rm eff}(\theta)$ and $g(\theta)$ and for the μ values required for the quadrature in expression (20). In practice, and in order to save computational time, we have interpolated from already available results for $I_\nu(\mu)$ (Kurucz 1996a, 1996b). These models assume a turbulence velocity of $2{\rm kms}^{-1}$. Although, following Castelli (1996), these models contain a conceptual error in the treatment of convection affecting color indices between 6000 K and 7500 K, we expect this to have little influence on our results, which are differential.

The values of β are obtained by interpolating to the grid in Tables 1 and 2 (see below) from the actual values indicated in Fig. 1 by triangles. In some cases, small extrapolations have been done.

The complete system of Geneva filters–B, U, V, $B1$, $B2$, $V1$ and G–has been considered. The response functions, $T_{\rm m}(\nu)$, were taken from Rufener & Nicolet (1988). We have extended the calculations to some Johnson filters–U, B and V–the passband functions being taken from Buser & Kurucz (1978)–see also Landolt-Börnstein (1982)–, and to filters u, v, b and y of the Strömgren system. For these filters the $T_{\rm m}(\nu)$ profiles are not standard but were taken from the Roque de los Muchachos Observatory (La Palma, Canary Islands, Spain), but since our results are differential, we believe that this is not of major importance.

In Tables 1 and 2 we give the resulting magnitude differences, as defined in Eq. (19), for solar metallicity. As shown below they can also be used for a wide range of metallicities to good accuracy. The values of $(T_{\rm e}, g_{\rm e})$ considered are as follow: $\log T_{\rm e}$ ($T_{\rm e}$ in K) goes from 3.80 to 4.04 in steps of 0.02 while $\log g_{\rm e}$ ($g_{\rm e}$ in ${\rm cm\ s^{-2}}$) goes from 3.30 to 4.35 in steps of 0.05. Note, however, that not all the possible pairs are included. In total there are 183 values of $(T_{\rm e}, g_{\rm e})$. Tests have shown that this grid is enough for further interpolations, to almost the accuracy reported in the tables. For each $(T_{\rm e}, g_{\rm e})$ we consider 9 values of $\tilde{w}$ (0.3, 0.5, 0.6, 0.7, 0.75, 0.8, 0.85, 0.9 and 0.95) and 10 values of i from 0° to 90° in steps of 10°. In the tables there are lines with the values of $\log T_{\rm e}$ and $\log g_{\rm e}$. After each of these, follow 90 lines with the corresponding values of $\tilde{w}$, i and the magnitude differences for the filters indicated at the top of each column.

In order to illustrate the kind of results given in Tables 1 and 2, we consider now three zero-age, zero-rotation models with solar metallicity and masses $1.5M_\odot$, $2.0M_\odot$ and $2.51M_\odot$. The points represented by asterisks in Fig. 2 correspond to the position of such non-rotating models in a colour–magnitude diagram in the Geneva system (the results are qualitatively similar if $B-V$ or $b-y$ colours are used instead of $B2-V1$). The position of these zero-rotation models was obtained by using the calibration explained in Sect. 3 below. Adding these magnitudes to the magnitude differences obtained by interpolating in Table 1, the corresponding magnitudes for rotating models can be found. In principle, we consider the same values of $T_{\rm e}$ and $g_{\rm e}$ for models with the same mass but different rotation rates. Changes in the interior structure caused by different rotation rates but otherwise fixed input physics will modify the values of L and $R_{\rm p}$ and hence those of $T_{\rm e}$ and $g_{\rm e}$, but for the moment we neglect such changes.

As commented at the beginning of Sect. 2, rotation makes the stars appear redshifted while the sign of the change in M_v depends on the angle of inclination i. This can be seen in Fig. 2. From the figure it follows that the change in colour $|\Delta(B2-V1)|$ can be as large as 0.1 and the change in magnitude $|\Delta M_v|$

Table 1. Magnitude differences between rotating and non-rotating copartners for a grid of models with solar metallicity. $T_{\rm e}$–given in K–and $g_{\rm e}$–given in $\rm cm\ s^{-2}$–are defined in Eqs. (22) and (21), respectively. Results are given for the filters in the Geneva system. To obtain the absolute magnitudes for a given rotating model, the magnitudes of a non-rotating model with $T_{\rm eff} = T_{\rm e}$, $g = g_{\rm e}$ and the same intrinsic luminosity must be added. (Only available in electronic form at the CDS).

$\log T_{\rm e}$	$\log g_{\rm e}$							
$\tilde{w}$	i	B	U	V	$B1$	$B2$	$V1$	G
3.80	3.60							
0.3	0.	-0.0081	-0.0067	-0.0149	-0.0059	-0.0103	-0.0147	-0.0160
0.3	10.	-0.0065	-0.0051	-0.0131	-0.0043	-0.0086	-0.0129	-0.0141
0.3	20.	-0.0044	-0.0030	-0.0119	-0.0021	-0.0068	-0.0116	-0.0131

Table 2. The same as Table 1 but for magnitude differences in the filters U, B and V of Johnson and the filters u, v, b and y of Strömgren. (Only available in electronic form at the CDS).

$\log T_{\rm e}$	$\log g_{\rm e}$							
$\tilde{w}$	i	U	B	V	u	v	b	y
3.80	3.60							
0.3	0.	-0.0059	-0.0099	-0.0149	-0.0061	-0.0076	-0.0122	-0.0150
0.3	10.	-0.0043	-0.0083	-0.0131	-0.0045	-0.0060	-0.0106	-0.0132
0.3	20.	-0.0022	-0.0064	-0.0119	-0.0024	-0.0038	-0.0089	-0.0120

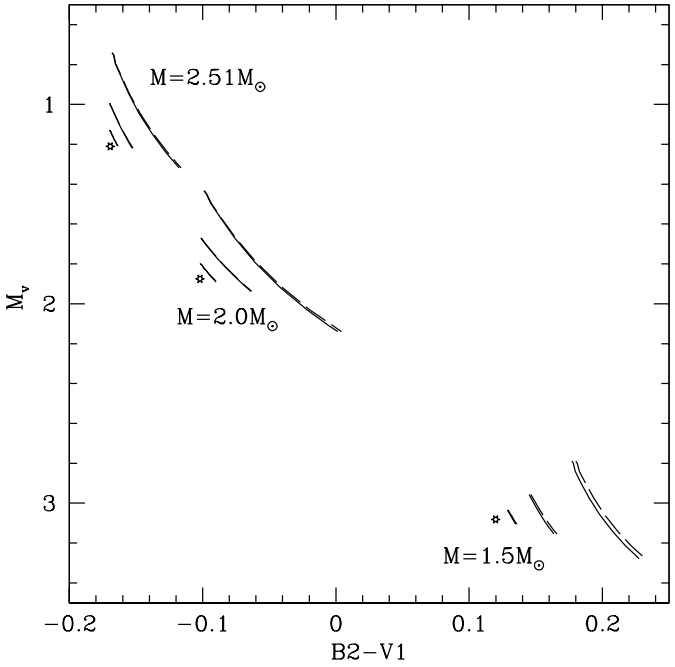

Fig. 2. Colour–magnitude diagram for rotating and non-rotating copartners for the three models indicated in the text. For each non-rotating model (indicated by an asterisk) there are three continuous lines corresponding to different values of $\tilde{w}$ that from left to right are 0.5, 0.75 and 0.95. Solar metallicity has been considered. Each line for constant $\tilde{w}$ runs from $i = 90^\circ$ (fainter model) to $i = 0^\circ$ (brighter model). The dashed lines are for models with the same parameters but $[M/H] = +0.2$.

as large as 0.45 for $\tilde{w} = 0.95$. However the effect is not linear in $\tilde{w}$, in particular for $\tilde{w} = 0.5$ the changes are much smaller: $|\Delta(B2 - V1)| < 0.02$ and $|\Delta M_v| < 0.1$. There are a large number of A and F stars with rotation rates $\tilde{w} > 0.5$ and for these stars the photometric effect of rotation cannot be neglected. It is also interesting to note the different behaviour for the $1.5M_\odot$ model, with a convective envelope and hence a low value of β, as compared to the $2.0M_\odot$ and $2.51M_\odot$ models with radiative envelopes and $\beta \simeq 1$.

A change in metallicity would modify these results in several ways. First, for the same age and masses, the interior structure and hence the global parameters of the models (L, R, etc...) change. Also, the location of the models in the colour–magnitude diagram changes if the calibration varies with metallicity. Finally, the atmospheric models are also different. To estimate the order of magnitude of this latter effect, we have calculated a table equivalent to Table 1 but with $[M/H] = +0.2$ ($Z \simeq 0.03$). The dashed lines in Fig. 2 corresponds to such a metallicity but keeping the position in the colour–magnitude diagram and the global parameters of the zero-rotation models fixed. It is clear that this effect is small for the $1.5M_\odot$ model, which has relatively important metallic lines, and it is almost negligible for the hotter models. Thus, Tables 1 and 2 can safely be used for metallicities of at least $Z = 0.03$, provided of course that suitable interior models and calibrations are used.

2.3. Effect due to changes in the interior structure

If non spherical interior rotating models are considered, then the procedure for computing the photometric parameters by using Tables 1 and 2 is straightforward. Only the corresponding values of $\tilde{w}$, $T_{\rm e}$ and $g_{\rm e}$ for each model considered, with given M, L, $R_{\rm p}$ and Ω, need to be considered.

The results given above can also be used for rotating models for which only the spherically symmetrical component of the

centrifugal force is taken into account. To calculate $\tilde{w}$, $T_{\rm e}$ and $g_{\rm e}$ for a given Ω, one needs, in addition to the values of the mass, M, and the intrinsic luminosity, L, of the model, an estimation of the polar radius, $R_{\rm p}$, of an equivalent, but shape distorted, model. To obtain this latter from the radius of the spherically symmetric rotating model, $R_{\rm ss}$, we note that, to leading order, the non spherical contributions to the structure quantities (ρ, p, ϕ,...) have a colatitude dependence proportional to $P_2(\cos\theta)$. These contributions are neglected in the spherically symmetric rotating models. Thus, it looks reasonable to take $R_{\rm ss} = R(\theta_0)$, where θ_0 is given by $P_2(\cos\theta_0) = 0$, that is, $\sin^2\theta_0 = 2/3$. In particular, in this way, Eq. (5) at θ_0 gives the same effective potential as the spherically symmetric rotating model. Hence, by using (Eq. 5) with $R(\theta_0) = R_{\rm ss}$ one finally get for the polar radius:

$$R_{\rm p} = \frac{R_{\rm ss}}{1 + \frac{\Omega^2 R_{\rm ss}^3}{3GM}} \ . \tag{23}$$

On the other hand, if one wishes to analyze a large set of models with different rotation rates (for instance in working with a cluster) or if rotating models are not available, then simple estimations of L and $R_{\rm p}$ can be obtained from their values for non-rotating models. To illustrate this point and to estimate the order of magnitude of this effect, we consider here the simple laws–see e.g. Tassoul (1978) and references therein:

$$L(w) = L(0)(1 - C_L w^2) \tag{24}$$

and

$$R_{\rm p}(w) = R_{\rm p}(0)(1 - C_R w^2) \ , \tag{25}$$

where $L(0)$ and $R_{\rm p}(0)$ refer to the non-rotating models and

$$w \equiv \frac{\Omega}{\Omega_{\rm c}} \ , \tag{26}$$

with

$$\Omega_{\rm c}^2 \equiv \frac{8GM}{27 R_{\rm pc}^3} \ . \tag{27}$$

Here $R_{\rm pc}$ is the polar radius a star with $w = 1$ would have, that is $R_{\rm pc} = R_{\rm p}(0)(1 - C_R)$. It can be shown that $\Omega_{\rm c}$ is the critical angular frequency (centrifugal force = gravity at the equator) for a family of uniformly rotating models of a given mass, for which Eq. (25) holds. Sackmann (1970) estimated $C_L = 0.055$ and $C_R = 0.013$ for a $2M_\odot$ model at the ZAMS. Other contemporaneous authors give similar results, see Tassoul (1978).

We can relate the relative angular velocity $\tilde{w}$ defined in Eq. (1) to the relative angular velocity w given in Eq. (26) by using Eq. (25):

$$\tilde{w}^2 = w^2 \left[\frac{1 - C_R w^2}{1 - C_R} \right]^3 \ . \tag{28}$$

The procedure for computing the magnitude differences are the same as in Sect. 2.2, but the values of $T_{\rm e}$ and $g_{\rm e}$ are computed for each $\tilde{w}$ by using Eqs. (28), (24) and (25).

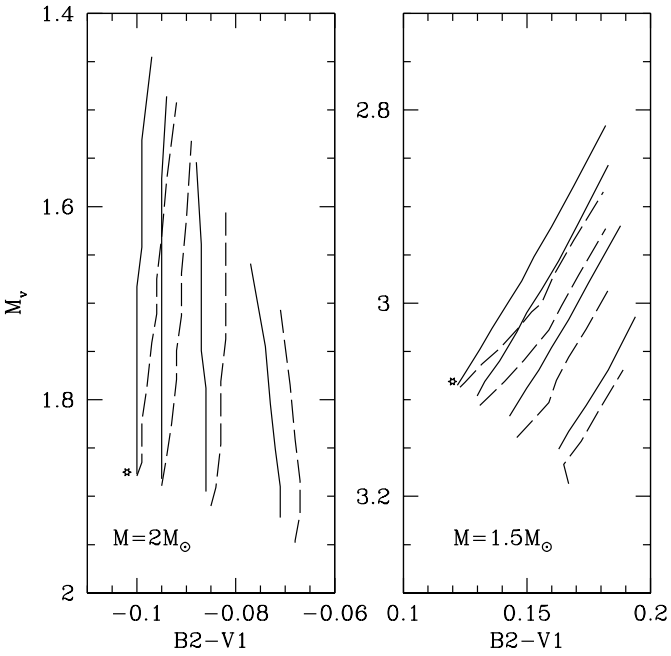

Fig. 3. Colour–magnitude diagrams for rotating models with different values of $v_{\rm e}\sin i$. The left panel is for a zero-age, solar-metallicity, $2M_\odot$ model and the right panel for a zero-age, solar-metallicity, $1.5M_\odot$ model. The continuous lines are for $C_L = C_R = 0$ while the dashed lines are for $C_L = 0.055$ and $C_R = 0.013$. Lines are for values $v_{\rm e}\sin i$ =50, 100, 150 and 200 $\mathrm{km\ s^{-1}}$ from left to right. Each line goes from $i = 90^\circ$ (bottom) to the value of i corresponding to $\tilde{w} = 0.95$ (top). The asterisks indicate the location of the non-rotating models.

To test the effect of the changes in the interior structure, we shall compare results obtained with the values of Sackmann for the coefficients C_L and C_R with those with $C_L = C_R = 0$. Since, based on spectroscopy observations, one can estimate the quantity $v_{\rm e}\sin i$, where $v_{\rm e}$ is the linear rotational velocity at the equator, we shall compare values at constant $v_{\rm e}\sin i$. For each $\tilde{w}$ in Table 1, the value of the equatorial radius is obtained from the radius of the non-rotating model by using Eqs. (25), (28), (3) and (4) with $\theta = \pi/2$. From this, we obtain $v_{\rm e}\sin i$ for the $\tilde{w}$ and i values in Table 1. The resulting magnitude differences are interpolated to some selected values of $v_{\rm e}\sin i$. Some results are shown in Fig. 3. The left panel is for the same $2M_\odot$ model as in Fig. 2 while the right panel shows the result for the $1.5M_\odot$ model. The continuous lines are for $C_L = C_R = 0$ and the dashed lines correspond to the values of Sackmann. In general, it can be seen an increase in M_v caused by the decrease in L when the Sackmann values for the coefficients are used. Also, the inclusion of the changes in the interior structure caused a larger redshift. This is mainly due to the fact that for a given $v_{\rm e}\sin i$ the corresponding relative angular velocity is larger for $C_R > 0$ than for $C_R = 0$, but the differences would be much smaller if compared at constant $\tilde{w}$.

The largest shift in colour is obtained for the largest $v_{\rm e}\sin i$, but at a first glance, it might seem strange that the largest change in M_v is achieved for the smallest $v_{\rm e}\sin i$. To interpret the figure

correctly we note that the computations are always carried out from the minimum value of $\tilde{w}$ up to $\tilde{w} = 0.95$, and that hence the lines of $v_{\rm e} \sin i = 50 {\rm km\,s^{-1}}$ contain the same maximum values of $\tilde{w}$ as those with $v_{\rm e} \sin i = 200 {\rm km\,s^{-1}}$ but for the former, in most cases, the star is seen pole-on and hence looks brighter. Of course, for randomly orientated objects, very large shifts for small $v_{\rm e} \sin i$ are unlikely.

We note also that for the $2M_{\odot}$ model the lines of constant $v_{\rm e} \sin i$ are roughly vertical. This means that the change in colour is essentially independent of i. This effect, that has interesting consequences for comparisons with observations where i is usually unknown, was first noticed by Maeder (1971) and holds as long as $\beta \simeq 1$. However Fig. 2 shows that for the $1.5M_{\odot}$ model, with $\beta \sim 0.3$, this is no longer valid.

We emphasize that the corrections due to interior changes given here are based on rotating models that include only dynamical changes in the stellar equations. If other aspects of rotation, such as mixing in the core, are considered, the situation can be very different, in particular for evolved models.

3. Non-rotating photometric counterparts for stars in a cluster

Here we address a problem that has already been confronted by Michel et al. (1999). We wish to have evolution models representative of several observed stars in a cluster, for instance of its δ Scuti stars. As a first step, isochrones must be fitted to exploit fully the advantages of using a cluster. Since each star has its own rotation rate, it is easier to search for Zero Rotation isochrones. Then, rather than compute photometric parameters for rotating models, we can try to translate the position of the observed stars in a colour–magnitude diagram to their non-rotating locations and fit the isochrones there. The non-rotating locations correspond to models with the same input physics as the rotating models, except that $\Omega = 0$. They were called "twin at rest" by Michel et al. (1999). Here they will be called non-rotating counterparts or associate models; they differ from the non-rotating copartners defined in Sect. 2.2 in that the former include changes in L and $R_{\rm p}$. Note that, since from observations one knows $v \sin i$ rather than w and i separately, the location of the non-rotating counterparts in the colour-magnitude diagram is not completely defined. Also, although the correction to the actual locations of the stars depends on the model considered, this dependence is not strong and in practice a simple iteration is enough to carry out a consistent correction.

3.1. Isochrones for the Praesepe Cluster

A good example to consider is the Praesepe Cluster. In this cluster, fast rotating F and A stars are located around the turning point. It is also a very interesting cluster for asteroseismology because 14 δ Scuti stars are known there. The metallicity of Praesepe is $Z = 0.02$–0.03 (Cayrel de Strobel et al. 1992) and the distance modulus as given by *HIPPARCOS* is $m_v - M_v = 6.24 \pm 0.12$ (Mermilliod et al. 1997). Geneva photometric data were taken from the catalogue of Rufener (1988) as distributed from the ADC. In general, the photometric errors are much smaller than the uncertainties in the shift caused by rotation and we shall neglect them. The reddening effect is negligible in Praesepe (Crawford & Barnes 1969).

Rotational velocities $v \sin i$ were taken from the revised catalogue of Uesugi & Fukuda (1982), also as distributed from the ADC. These $v \sin i$ values are calculated in the old Slettebak system, which does not take into account the dynamical effect of fast rotation in the atmospheric models. Although, as mentioned in the introduction, Slettebak et al. (1975) did consider the dynamical effect of rotation on the spectral lines, to our knowledge there are no available data in this system for a whole set of stars in Praesepe. Even noting that there can be important systematic errors, we shall use the results of Uesugi & Fukuda (1982) and assume that the quantity $v \sin i$ derived from observations is in fact $v_{\rm e} \sin i$.

Isochrones suitable for the Praesepe Cluster have been computed using the code and input physics described in Claret (1995). The value of the overshooting parameter considered here is $\alpha_{\rm ov} = 0.2$. We have taken two metallicities, $Z = 0.02$ and $Z = 0.027$, and ages in the range 0.6Gy to 0.8Gy. These isochrones were then transformed to a M_v–$(B2-V1)$ diagram by using the calibration of Künzli et al. (1997) for $B2 - V1$ (which is based on $T_{\rm eff}$ and g and gives at the same time the value of the Geneva photometric parameter d) and the calibration of Schmidt-Kaler (1982) for M_v. As an example, the thin continuous line in Fig. 4 corresponds to an isochrone with $Z = 0.02$ and $t = 0.8$Gy. Only the colour–magnitude diagram around the turning point is shown. For this cluster there is no problem in fitting the lower part of the diagram using the distance given by *HIPPARCOS*.

In Fig. 4 we also show the actual position of the Praesepe stars with known $v \sin i$ (after rejecting those catalogued as binary) and the position of their non-rotating counterparts. A distance modulus of 6.24 has been used. To obtain these counterparts, specific models must be used. After a simple iteration, we choose for each star the model on the isochrone that is closest to the corresponding non-rotating counterpart. In any case, the resulting "correction" is very similar if a neighbouring model on the isochrone is used.

From Fig. 4 it can be seen that if the effect of rotation were neglected, the age of the cluster determined on the basis of an isochrone fit would be overestimated by a few hundred million years. We find that with a value of $\alpha_{\rm ov} = 0.2$ for the overshooting parameter, the best fits are obtained for an age of t =0.75–0.85 Gy if a metallicity of $Z = 0.02$ is considered and an age of t=0.6–0.7 Gy for $Z = 0.027$. These values are roughly similar to those found by Michel et al. (1999), also after correcting for the effect of rotation.

A second point to be discussed is the dispersion of the stars in the colour–magnitude diagram. It can be seen that the actual position of the stars around the turning point cannot be completely matched by a single isochrone. However, the effect of rotation is larger than this and, potentially, could remove such a scatter. Unfortunately, we do not known the angle of inclination i for each star and hence we cannot convincingly check if this is

in fact true. On the other hand, it seems clear that alternative explanations for this dispersion, such as small differences in age or metallicity or unknown binaries remaining in the data set, cannot be based on photometric diagrams containing fast rotators such as the colour–magnitude (or a colour–colour) diagram of Praesepe around the turning point.

A further insight can be achieved by considering that the stars in the cluster should be randomly orientated. Collins & Smith (1985) carried out a detailed theoretical analysis on this issue. Although beyond the scope of our work, we wish to mention a simple point because at first sight it could be thought, by looking at Fig. 4, that at least for $B2-V1>0$ the scatter induced by rotation could be larger than the actual dispersion in the cluster. However this is not true because not all the points on the lines corresponding to the location of the non-rotating counterparts are equally probable. The thick continuous lines in Fig. 4 give the non-rotating counterparts but constrained to angles of inclination greater than about 32° ($\cos i$ smaller than about 0.85). Approximately 85% of the stars (21 out of 25 in the figure) must have angles in this range. As can be seen in the figure, the average shift induced by rotation for this range of i is much smaller.

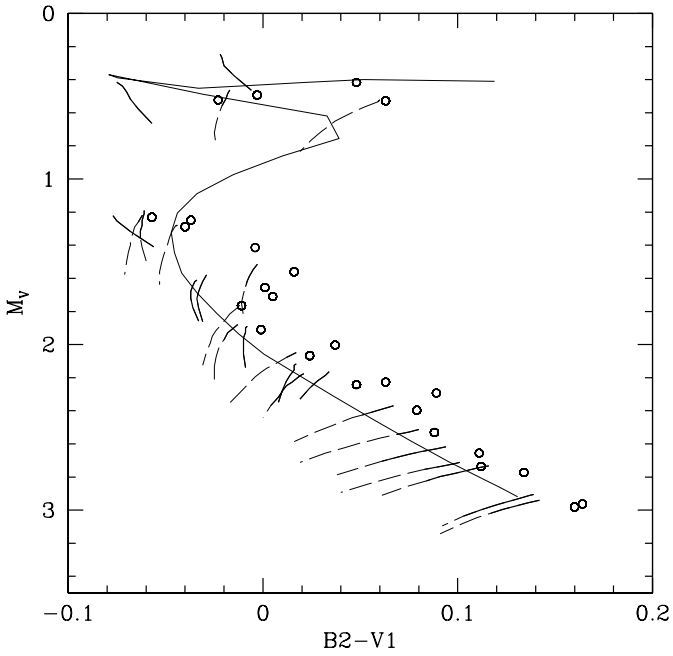

Fig. 4. Colour–magnitude diagram for the Praesepe Cluster. Only the region around the turning point is shown. The open circles correspond to the actual location of the stars with known $v\sin i$. Stars catalogued as binaries were rejected. The thin continuous line is an isochrone with $\alpha_{\rm ov}=0.2$, $Z=0.02$ and an age of 0.8Gy. The dashed lines give the location of the non-rotating counterparts when using the reported values of $v\sin i$ and changing the angle of inclination from $i=90^\circ$ to that value corresponding to $\tilde{w}=0.95$. The thick continuous lines are the same but limited to, approximately, angles i greater than 32°. Approximately 85% of the stars must have angles in this range.

3.2. Non-rotating associate models for the δ Scuti stars in the Praesepe Cluster

In this section we shall estimate the range of stellar parameters for non-rotating associate models, but restricted to the 14 δ Scuti stars in the cluster. In principle, these counterparts are useful only if non-rotating models with the same mass and evolved stage as the rotating models are required. At the end of the section we give some comments for the case of spherically symmetric rotating models.

Within the framework of the method described in previous sections, we believe that the most important sources of uncertainties are the determination of $v\sin i$ and the parameters of the models (mainly the radius but also the luminosity, mass and composition) chosen for computing the non-rotating counterparts.

Regarding the determination of $v\sin i$ we shall assume errors of $\pm 10{\rm kms}^{-1}$. This value can be considered typical for different measurements of the same star using the same method for estimating $v\sin i$, but it does not include the systematic uncertainty caused by using this technique, developed for slowly rotating stars. As indicated above, for some stars, especially when $v\sin i\simeq 200{\rm km\ s}^{-1}$, this latter error can be larger than that considered here.

On the other hand, for estimating the uncertainty coming from the model parameters, we have used two isochrones with values $t=0.8$Gy, $Z=0.02$ and $t=0.6$Gy, $Z=0.027$. These isochrones have rather extreme values of Z for Praesepe and to them correspond for each star two different non-rotating counterparts that allow an estimate to be made of the order of magnitude of the uncertainties in the results coming from the choice of model parameters. To this, one should add the uncertainties from changes in the interior structure of the rotating models. We have limited our work to the use of Eqs. (24) and (25). We have checked that changing the coefficients C_R and C_L from those of Sackmann (1970) to those of Papaloizou & Whelan (1973), the differences in the estimation of the stellar parameters for the non-rotating counterparts are clearly smaller than when comparing results using models from the two isochrones. Of course other possible effects of rotation on the models can introduce larger uncertainties than those considered here.

In Fig. 5 we show the position of the δ Scuti stars in a colour–magnitude diagram. For clarity we have divided the figure into four panels. The open circles are the actual positions of the stars using a distance modulus of 6.24. For each star there are four continuous lines corresponding to non-rotating associate models. These four lines are obtained by using the corresponding models from the two isochrones mentioned above and for each of them, two values of the projected velocity: $v\sin i+10{\rm km\ s}^{-1}$ and $v\sin i-10{\rm km\ s}^{-1}$.

It can be seen that the lines of the non-rotating models are grouped in pairs that, except for KW284 (with the smallest velocity, $v\sin i=30{\rm km\ s}^{-1}$), are for given projected velocity. The lines with $v\sin i+10{\rm km\ s}^{-1}$ are on the left and those with $v\sin i-10{\rm km\ s}^{-1}$ are on the right. Thus, in general, the error in $v\sin i$ seems to be the largest source of uncertainty.

In Table 3 we give the range of stellar parameters for the 14 δ Scuti stars. For each star we give in a first line the KW number, the rotation velocity $v \sin i$, the apparent visual magnitude, m_v, the colour index, $B2-V1$, and the photometric parameter d. Then follow $(T_{\rm eff})_{\rm phot}$, $\log g_{\rm phot}$ and $(L/L_\odot)_{\rm phot}$. The quantities $(T_{\rm eff})_{\rm phot}$ and $\log g_{\rm phot}$ correspond to the values derived from $B2-V1$ and d as given by the calibration of Künzli et al. (1997) for $[M/H] = +0.2$ (the smallest values for both quantities) and $[M/H] = 0$ (the largest values). The quantity $(L/L_\odot)_{\rm phot}$ was obtained from m_v by using the Schmidt-Kaler (1982) calibration and a distance modulus of 6.24. Thus $(T_{\rm eff})_{\rm phot}$, $\log g_{\rm phot}$ and $(L/L_\odot)_{\rm phot}$ are respectively the values of $T_{\rm eff}$, $\log g$ and $L/L_\odot$ that a non-rotating star with the same photometric parameters would have. However, since we are considering fast-rotating stars, they have not an intrinsic meaning.

The next lines for each star in Table 3 contain the stellar parameters of the non-rotating associate models, depending on the values of $\tilde{w}$ and i of the actual stars. We consider several values of $\tilde{w}$. The first one is the minimum for which we give its range, depending on $v \sin i$ and the model considered. Then follow results for fixed $\tilde{w}$. We give for each $\tilde{w}$, the corresponding range of values of the cyclic rotational frequency $\nu_{\rm rot}$, the angle of inclination, i, and the range of values of $T_{\rm eff}$, $\log g$ and $L/L_\odot$ for the non-rotating associate models. Here, after correcting m_v, $B2-V1$ and d for rotation, we use the same calibrations as above.

Note that the range of values given in Table 3 corresponds only to the uncertainties inherent to the effects mentioned at the beginning of this section, but other errors can be considered separately. For instance, the value of $L/L_\odot$ has in addition an uncertainty associated with the error in the distance which is the same for all the stars in the cluster. Also, the absolute values reported in Table 3 depend on the calibration used. For instance, the uncertainty in $T_{\rm eff}$ due to the calibration can be as large as 100K, but the differential results, e.g. $T_{\rm eff} - (T_{\rm eff})_{\rm phot}$, should be little dependent on this and hence can still be used if the value of e.g. $(T_{\rm eff})_{\rm phot}$ is replaced by that given by a different calibration.

From Table 3 follows that if non-rotating models are considered and the effect of rotation were neglected, the value of $T_{\rm eff}$ obtained from a photometric calibration would be smaller by a size that for most of the stars considered here would be more than 100K, and could be even bigger than 450K in some extreme cases (for KW207). The luminosity of the non-rotating associate models depends strongly on the angle of inclination. For stars seen equator-on ($i \simeq 90°$), the luminosity of the non-rotating models can be larger by 20% than the one that would be obtained if no correction were applied (that is than $(L/L_\odot)_{\rm phot}$). For stars seen pole-on, the luminosity of the associate models can be smaller by 25% compared to $(L/L_\odot)_{\rm phot}$.

In performing an asteroseismological analysis one usually compares mode frequencies of given models with those observed. For fast-rotating stars, such as δ Scuti stars, the frequencies (including those of radial modes) depend strongly on the value of the rotational frequency $\nu_{\rm rot}$. To each range of $\nu_{\rm rot}$ a different range of $T_{\rm eff}$ and mainly of $L/L_\odot$ are associated as shown in Table 3. Thus, although the global uncertainty in $L/L_\odot$ for a given star is large, a consistent asteroseismological analysis should not deal with such global uncertainties. This was the reason for giving such detailed results in Table 3.

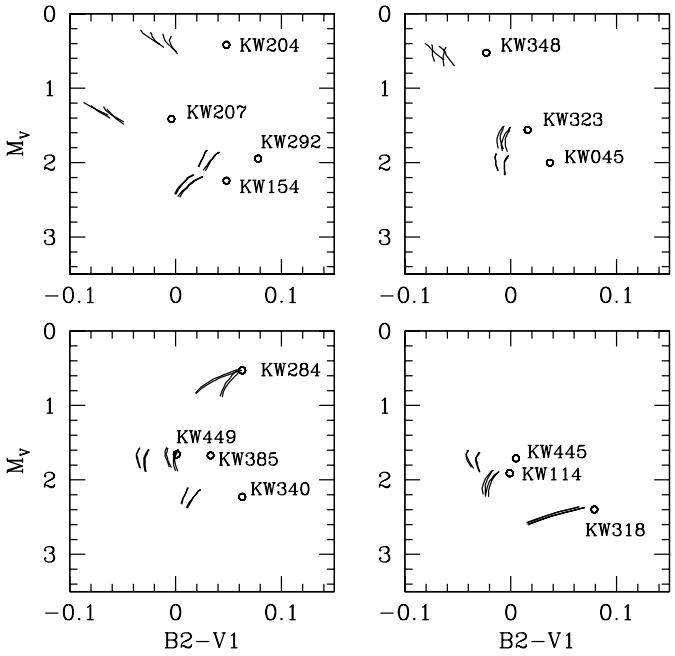

Fig. 5. Colour–magnitude diagram for the δ Scuti stars in the Praesepe Cluster. The open circles correspond to the actual location of the stars. Their name in the KW nomenclature is indicated. The continuous lines give the location of the non-rotating associate models limited to $\tilde{w} = 0.95$ for the relative angular rotation. Two isochrones and two values for the projected velocity, as detailed in the text, have been considered.

In Michel et al. (1999) and Hernández et al. (1998) not such detailed corrections were considered. On the other hand, since they used conservative error bars in the location of the position of the stars in the colour-magnitude diagram, no relevant changes in their conclusions are expected.

If, in the computation of zero and first order frequencies, spherically symmetric rotating models are used instead of non-rotating models (as for instance in Kjeldsen et al. 1998 and Soufi et al. 1998), one has a similar problem albeit less severe for $T_{\rm eff}$. Although in this case the best is to perform all the computations by using Tables 1 and 2 and the corresponding models, simple estimations can be done for their stellar parameters, as required by the photometric observations, by noting that the luminosity of such models would have similar ranges to those reported in Table 3 and that for $T_{\rm eff}$ and g one can use Eqs. (23) and (25)–even with $C_R = 0$–for rescaling the radius and hence $T_{\rm eff}$ and g in Table 3. The resulting $T_{\rm eff}$ should be, in most of the cases, closer to $(T_{\rm eff})_{\rm phot}$.

4. Conclusions

We have computed the photometric magnitudes of rotating models for a grid suitable for main sequence and slightly evolved

Table 3. Non-rotating associate models for the δ Scuti stars in the Praesepe cluster. $\nu_{\rm rot}$ is given in μHz, $T_{\rm eff}$ in K and g in $\mathrm{cm\ s^{-2}}$. See text for details.

	$v \sin i$	m_v $\tilde{w}$	$B2-V1$ $\nu_{\rm rot}$	d i	$(T_{\rm eff})_{\rm phot}$ $T_{\rm eff}$	$\log g_{\rm phot}$ $\log g$	$(L/L_\odot)_{\rm phot}$ $L/L_\odot$
KW204	150.	6.657	0.048	1.349	7210–7220	3.63–3.71	48.9
		0.70–0.81	7.8–8.5	90	7510–7680	3.63–3.67	54.6–58.7
		0.85	9.2- 9.6	51–68	7520–7680	3.64–3.70	49.7–56.5
		0.95	11.3–11.8	39–49	7510–7630	3.73–3.79	43.6–49.1
KW348	145.	6.763	–0.023	1.422	7730–7760	3.88–3.94	44.3
		0.64–0.75	9.9–11.6	90	8040–8280	3.86–3.94	47.6–49.8
		0.85	13.0–14.0	49–57	8080–8210	3.87–3.97	42.5–46.3
		0.95	15.0–16.5	34–43	8040–8160	3.89–4.02	37.5–40.5
KW284	30.	6.768	0.063	1.306	7140–7150	3.67–3.75	44.14
		0.11–0.22	1.2–2.7	90	7140–7170	3.68–3.75	44.3–44.5
		0.5	5.7–6.1	12–25	7170–7210	3.69–3.73	42.1–42.9
		0.85	10.1–10.4	6–13	7250–7330	3.73–3.73	35.7–37.5
		0.95	11.8–12.3	5–10	7280–7410	3.77–3.78	31.6–33.5
KW207	200.	7.654	–0.004	1.313	7720–7750	4.11–4.17	19.52
		0.77–0.84	18.3–19.4	90	8220–8430	4.04–4.13	22.1–23.9
		0.85	18.4–21.0	60–82	8180–8410	4.04–4.13	20.8–23.7
		0.95	24.0–25.0	45–54	8090–8230	4.15–4.21	18.2–20.5
KW323	115.	7.801	0.016	1.257	7620–7650	4.18–4.24	17.04
		0.45–0.53	12.9–16.2	90	7740–7800	4.20–4.26	17.6–17.9
		0.6	17.5–18.3	46–61	7750–7820	4.21–4.25	16.9–17.6
		0.85	25.1–26.0	28–34	7780–7850	4.22–4.25	14.7–15.4
		0.95	29.0–30.0	22–27	7780–7860	4.24–4.28	13.0–13.6
KW449	145.	7.896	0.001	1.300	7690–7720	4.12–4.19	15.62
		0.56–0.64	15.2–18.1	90	7880–7970	4.13–4.19	16.5–17.0
		0.7	19.0–20.0	50–64	7890–7980	4.13–4.19	16.4–16.6
		0.85	23.1–24.2	36–44	7910–7990	4.13–4.19	14.3–15.0
		0.95	27.2–28.1	29–34	7920–7990	4.17–4.22	12.6–13.2
KW445	165.	7.950	0.005	1.248	7750–7770	4.28–4.34	14.86
		0.63–0.71	21.3–25.0	90	7990–8110	4.26–4.35	16.1–16.5
		0.7	21.9–23.4	62–88	8000–8100	4.26–4.35	15.6–16.5
		0.85	26.8–28.1	43–52	8010–8110	4.26–4.34	14.2–15.1
		0.95	31.9–32.4	34–40	8010–8090	4.31–4.36	12.5–13.3
KW114	95.	8.150	–0.001	1.230	7830–7860	4.37–4.43	12.36
		0.36–0.45	12.4–16.0	90	7900–7970	4.37–4.43	12.6–12.8
		0.5	17.9–19.0	46–63	7920–7990	4.37–4.43	12.3–12.7
		0.85	30.7–32.3	22–28	7980–8040	4.38–4.42	10.4–10.8
		0.95	35.4–37.0	18–22	7990–8060	4.40–4.44	9.2–9.5
KW045	170.	8.243	0.037	1.204	7510–7530	4.22–4.29	11.34
		0.65–0.72	20.2–23.2	90	7760–7850	4.20–4.25	12.4–12.8
		0.85	26.1–27.8	44–52	7800–7870	4.22–4.28	11.0–11.7
		0.95	31.0–32.6	35–40	7810–7880	4.28–4.32	9.7–10.3
KW340	170.	8.467	0.063	1.191	7290–7310	4.09–4.16	9.23
		0.65–0.71	17.9–21.1	90	7530–7620	4.07–4.13	10.1–10.3
		0.85	23.2–24.7	44–52	7590–7650	4.11–4.16	9.0–9.5
		0.95	27.2–28.9	35–40	7640–7700	4.15–4.20	8.0–8.5
KW154	135.	8.482	0.048	1.179	7450–7470	4.23–4.30	9.10
		0.52–0.60	16.1–19.0	90	7590–7660	4.23–4.29	9.6–9.8
		0.7	21.7–23.1	45–55	7630–7690	4.22–4.26	9.1–9.4
		0.85	27.1–28.7	33–39	7690–7750	4.24–4.29	8.3–8.7
		0.95	31.4–33.1	26–31	7750–7800	4.27–4.32	7.4–7.7

Table 3. (continued)

	$v \sin i$	m_v $\tilde{w}$	$B2-V1$ $\nu_{\rm rot}$	d i	$(T_{\rm eff})_{\rm phot}$ $T_{\rm eff}$	$\log g_{\rm phot}$ $\log g$	$(L/L_\odot)_{\rm phot}$ $L/L_\odot$
KW318	100.	8.637	0.079	1.130	7240–7260	4.21–4.28	7.89
		0.38–0.46	11.7–15.3	90	7300–7350	4.22–4.29	8.1–8.2
		0.5	15.9–17.3	49–66	7330–7360	4.22–4.29	7.9–8.1
		0.85	27.4–29.6	23–29	7520–7550	4.23–4.29	7.1–7.3
		0.95	31.5–34.1	19–23	7660–7690	4.25–4.32	6.5–6.7
KW292	165.	8.188	0.078	1.164	7200–7220	4.08–4.16	11.93
		0.63–0.70	16.4–19.0	90	7410–7500	4.06–4.12	12.9–13.3
		0.7	18.0–19.2	61–86	7435–7500	4.06–4.12	12.6–13.3
		0.85	23.0–24.4	42–50	7480–7540	4.10–4.15	11.5–12.1
		0.95	26.8–28.7	34–39	7530–7590	4.15–4.19	10.3–10.8
KW385	155.	7.911	0.033	1.211	7530–7560	4.22–4.29	15.40
		0.60–0.67	18.3–21.0	90	7740–7830	4.24–4.28	16.5–17.0
		0.7	21.6–22.6	56–70	7760–7840	4.24–4.28	15.8–16.7
		0.85	26.3–27.8	39–47	7780–7850	4.24–4.29	14.4–15.2
		0.95	31.2–32.6	31–37	7780–7850	4.29–4.32	12.6–13.3

stars of spectral type A0 to F5. The location of the stars in a colour–magnitude diagram depends not only on the angular velocity, Ω, but also on the angle of inclination, i. The general results are given in Tables 1 and 2 as magnitude differences between rotating and non-rotating copartners since in this way they are independent of any photometric calibration.

For the hotter models with radiative envelopes and hence gravity-darkening exponent $\beta \approx 1$, the results are qualitatively similar to those found previously by other authors (e.g. Maeder & Peytremann 1970; Collins & Smith 1985), who assumed the von Zeipel gravity-darkening law ($\beta = 1$), but the atmospheric models considered here have an updated physics. Also, the grid of models considered in the present work is much more extensive. Although, in addition, we have considered different metallicities, we have found that for $[M/H] = +0.2$ the magnitude differences are very similar to those with $[M/H] = 0$ and hence we give only results for solar metallicity. For the cooler models with convective envelopes we have found a qualitatively different behaviour after using a general gravity-darkening law and, in this sense, the results can be considered as new.

When non-spherical rotating models are available, the results in Tables 1 and 2 can be used in a straightforward way, but we have also illustrated its use when spherically symmetric, rotating or non-rotating, models are considered. The effect of changes in the internal structure (namely, in the intrinsic luminosity, L, and the polar radius, $R_{\rm p}$) due to rotation cannot be neglected, though they are in general clearly smaller than the effect of shape distortion and gravity-darkening.

We have investigated the problem of obtaining non-rotating associate models for the stars in a cluster. This is useful in investigations where non-rotating models are used but yet one is still dealing with fast rotating stars. For the δ Scuti stars in the Praesepe Cluster, if non-rotating models are used and no correction for rotation is applied, the value of $T_{\rm eff}$ obtained from a photometric calibration would be smaller by a few hundred degrees than its value after such a correction. The luminosity of the non-rotating associate models depends strongly on the angle of inclination. For stars seen equator-on ($i \simeq 90^\circ$) the luminosity of the non-rotating models can be larger by 20% than would be obtained if no correction were applied. For stars seen pole-on, the luminosity of the associate models can be smaller by 25%. Qualitatively similar results were found by Michel et al. (1999), who used the computations by Maeder & Peytremann (1970).

Even though after correcting for rotation, and because the angle of inclination, i, is unknown, one obtains a significant increase in the luminosity uncertainty, it must be borne in mind that, if $v_{\rm e} \sin i$ is fixed by observations, other parameters, such as the cyclic rotational frequency, $\nu_{\rm rot}$, also depend on i. This correlation is in particular interesting when comparing theoretical and observed frequencies of oscillation.

Acknowledgements. We are grateful to C. Allende, A. Alonso, J. Christensen-Dalsgaard, H. Kjeldsen and B. Ruiz Cobo for fruitful discussions. We are also grateful to our referee, R.C. Smith, who has helped in enlighting the paper.

References

Annamma M., Rajamohan R., 1992, J. Astrophys. Astr. 13, 61
Buser R., Kurucz R.L., 1978, A&A 70, 555
Carpenter K.G., Slettebak A., Sonneborn G., 1984, ApJ 286, 741
Castelli F., 1996, In: Adelman S.J., Kupka F., Weiss W.W. (eds.) Model Atmospheres and Spectrum Synthesis. Proceedings of the 5th Vienna International Workshop, ASP Conference Series, Vol. 108, p. 85
Cayrel de Strobel G., Hauck B., François P., et al., 1992, A&AS 95, 273
Claret A., 1995, A&AS 109, 441
Claret A., 1998, A&AS 131, 395
Collins G.W. II, 1963, ApJ 138, 1134
Collins G.W. II, 1965, ApJ 142, 265
Collins G.W. II, 1966, ApJ 146, 914

Collins G.W. II, 1974, ApJ 191, 157
Collins G.W. II, Smith R.C., 1985, MNRAS 213, 519
Collins G.W. II, Sonneborn G.H., 1977, ApJS 34,41
Crawford D.L., Barnes J.V., 1969, AJ 74, 818
Figueras F., Blasi F., 1998, A&A 329, 957
Hardorp J., Strittmatter P.A., 1968, ApJ 151, 1057
Harrington J.P., Collins G.W. II, 1968, ApJ 151, 1051
Hernández M.M., Pérez Hernández F., Michel E., et al., 1998, A&A 338, 511
Kjeldsen H., Arentoft T., Bedding T.R. et al., 1998, In: Korzennik S.G., Wilson A. (eds.) Structure and dynamics of the interior of the Sun and Sun-like stars. Proc. SOHO 6/GONG 98 Workshop, ESA SP-418, in press
Kurucz R.L., 1996a, Kurucz CD-ROM No. 16, Smithsonian Astrophys. Obs.
Kurucz R.L., 1996b, Kurucz CD-ROM No. 17, Smithsonian Astrophys. Obs.
Künzli M., North P., Kurucz R.L., Nicolet B., 1997, A&AS 122, 51
Landolt-Börnstein, 1982, New Series, Vol. VI/2b, Springer-Verlag
Lucy L.B., 1967, Zeitschritft für Astrophysik 65, 89
Maeder A., 1971, A&A 10, 354
Maeder A., Peytremann E., 1970, A&A 7, 120
Maeder A., Peytremann E., 1972, A&A 21, 279
Mermilliod J.C., Turon C., Robichon N., Arenou F., Lebreton Y., 1997, In: Hipparcos Venice '97, ESA SP-402, 643
Michel E., Hernández M.M., Baglin A., Lebreton Y., Belmonte J.A. 1998, In: Bradley P.A., Guzik J.A. (eds.) ASP Conf Series vol. 135, 475
Michel E., Hernández M.M., Houdek G., et al., 1999, A&A 342, 153
Papaloizou J.C., Whelan J.A.J., 1973, MNRAS 164, 1
Rufener F., 1988, Catalogue of Stars Measured in the Geneva Observatory
Rufener F., Nicolet B., 1988, A&A 206, 357
Sackmann I.-J., 1970, A&A 8, 76
Schmidt-Kaler Th., 1982, In: Landolt-Börnstein New Series VI/2b, Springer-Verlag, 451
Shajn G., Struve O., 1929, MNRAS 89, 222
Slettebak A., Collins G.W. II, Boyce P.B., White N.M., Parkinson T.D., 1975, ApJS 29,137
Smith R.C., 1970, MNRAS 148, 275
Smith R.C., Worley R., 1974, MNRAS 167, 199
Soufi F., Goupil M.J., Dziembowski W.A., 1998, A&A 334, 911
Tassoul J.-L., 1978, Theory of Rotating Stars. Princeton Series in Astrophysics, Princeton University Press
Uesugi A., Fukuda I., 1982, Revised Cat. of Stellar Rotational Velocities, Kyoto University